JACC Vol. 15, No. 5
April 1990:1032–42

Noninvasive Quantification of Regional Blood Flow in the Human Heart Using N-13 Ammonia and Dynamic Positron Emission Tomographic Imaging

GARY D. HUTCHINS, PHD,* MARKUS SCHWAIGER, MD,* KAREN C. ROSENSPIRE, PHD,* JANINE KRIVOKAPICH, MD, FACC,† HEINRICH SCHELBERT, MD, FACC,† DAVID E. KUHL, MD*

Ann Arbor, Michigan and Los Angeles, California

Evaluation of regional myocardial blood flow by conventional scintigraphic techniques is limited to the qualitative assessment of regional tracer distribution. Dynamic imaging with positron emission tomography allows the quantitative delineation of myocardial tracer kinetics and, hence, the measurement of physiologic processes such as myocardial blood flow. To test this hypothesis, positron emission tomographic imaging in combination with N-13 ammonia was performed at rest and after pharmacologically induced vasodilation in seven healthy volunteers.

Myocardial and blood time-activity curves derived from regions of interest over the heart and ventricular chamber were fitted using a three compartment model for N-13 ammonia, yielding rate constants for tracer uptake and retention. Myocardial blood flow (K_1) averaged 88 ± 17 ml/min per 100 g at rest and increased to 417 ± 112 ml/min per 100 g after dipyridamole infusion (0.56 mg/kg) and handgrip exercise. The coronary reserve averaged 4.8 ± 1.3 and was not significantly different in the septal, anterior and lateral walls of the left ventricle. Blood flow values showed only a minor dependence on the correction for blood metabolites of N-13 ammonia.

These data demonstrate that quantification of regional myocardial blood flow is feasible by dynamic positron emission tomographic imaging. The observed coronary flow reserve after dipyridamole is in close agreement with the results obtained by invasive techniques, indicating accurate flow estimates over a wide range. Thus, positron emission tomography may provide accurate and noninvasive definition of the functional significance of coronary artery disease and may allow the improved selection of patients for revascularization.

(J Am Coll Cardiol 1990;1032–42)

Noninvasive approaches to define the effect of coronary artery disease on regional myocardial blood flow using accurate quantitative flow measurements in human patients may enhance our understanding of disease processes and improve subsequent treatment strategies. Sophisticated techniques available in the animal model (1) allow the quantitative assessment of regional myocardial blood flow under a variety of experimental conditions. Most of these techniques are invasive (flow probes) or require the postmortem analysis of tissue radioactivity (radiolabeled microspheres). Therefore, transfer of these technologies to the human heart is limited. Several imaging approaches have recently been introduced (2–5) to qualitatively evaluate myocardial blood flow; these include radionuclide methods, echocardiography, nuclear magnetic resonance imaging and dynamic X-ray computed tomography. Thallium-201 scintigraphy represents the most widely used noninvasive approach to assess myocardial blood flow (2,5). It provides high diagnostic accuracy for the identification of coronary artery disease, but can detect only relative blood flow abnormalities. In addition, the low photon energy of thallium-201 results in significant photon attenuation by tissue surrounding the heart, which degrades the

From the *Department of Internal Medicine, Division of Nuclear Medicine, University of Michigan Medical Center, Ann Arbor, Michigan and the †Division of Nuclear Medicine and Biophysics, Laboratory of Biomedical and Environmental Sciences, University of California-Los Angeles School of Medicine, Los Angeles, California. This study was supported by the American Heart Association of Michigan, Ann Arbor (Grant 88-0699-J1) and by the National Institutes of Health (Grants HL29845, HL33177 and HL25625), Bethesda, Maryland.

Manuscript received June 7, 1989; revised manuscript received November 8, 1989, accepted November 21, 1989.

Address for reprints: Gary D. Hutchins, PhD, University of Michigan Medical Center, 3480 Kresge III Building, Box 0552, Ann Arbor, Michigan 48109-0552.

0735-1097/90/$3.50

image quality and the specificity of tracer uptake abnormalities.

Several positron-emitting tracers for assessment of myocardial blood flow have been introduced for positron emission tomography (6–8). Freely diffusible tracers such as O-15 water are suitable for the measurement of myocardial blood flow, but require sophisticated imaging protocols with subtraction of blood pool activity (7,9,10). N-13 ammonia and rubidium-82 have been employed as "chemical microspheres" for the measurement of myocardial blood flow (11–14). However, even though high quality images are attainable, the retention of these radiopharmaceuticals is incomplete, resulting in a nonlinear relation between tissue radionuclide accumulation and blood flow. Previous animal and clinical studies (13,14) with N-13 ammonia and positron emission tomography have shown the feasibility of qualitative and quantitative estimates of myocardial blood flow. However, the quantification of blood flow with N-13 ammonia has been limited by the flow-dependent decrease in retention as the blood flow increases (14).

Although N-13 ammonia is highly extracted by myocardial tissue, its myocardial retention depends on its metabolic incorporation into glutamine (6,15). By using dynamic positron emission tomographic scanning with high temporal resolution and tracer kinetic modeling, the separation of initial tracer extraction and subsequent metabolic conversion to glutamine can be achieved. Blood flow measurements based on initial myocardial N-13 ammonia uptake rather than net retention are expected to expand the dynamic range of measurable myocardial flood flow. In this study we tested this hypothesis using dynamic positron emission tomographic imaging and a three-compartment model describing N-13 ammonia kinetics in the human heart at rest and after pharmacologically induced coronary vasodilation.

Methods

Study subjects. Seven healthy human volunteers free of cardiovascular disease as assessed by history and physical examination participated in this investigation. The mean age was 24 ± 4 years. All subjects were studied under fasting conditions (>12 h). After giving informed, written consent, each subject was positioned in the ECAT-911 (CTI) whole body scanner for image acquisition.

Positron emission tomography. A rectilinear scan was performed to localize the heart and define the position of the detector rings over the heart silhouette for the acquisition of transmission images. Transmission images were acquired for 10 min and subsequently used to generate attenuation correction factors. Ten millicuries of N-13 ammonia was injected intravenously as a slow bolus over 30 s using a Harvard infusion pump (Gould, Inc.). Simultaneously, dynamic image acquisition was initiated with varying frame durations. Twelve 10 s frames were followed by four 30 s frames and one 360 s frame. The total acquisition time after injection of N-13 ammonia was 10 min. After acquisition of the baseline study, a period of 50 min was allowed for the physical decay of N-13 (physical half-life 9.9 min).

Figure 1. Three compartment tracer kinetic model describing extraction and retention of N-13 ammonia in myocardial tissue. K_1 and k_2 reflect exchange of N-13 ammonia between vascular and extravascular space in the myocardium, and k_3 represents metabolically (METABOL.) trapped N-13 ammonia in the form of glutamine.

Dipyridamole (0.56 mg/kg) was infused intravenously over 4 min. After an additional 4 min, the volunteer was asked to perform handgrip exercise for 4 min at 50% maximal strength (16). The second injection (30 s bolus) of 10 mCi of N-13 ammonia was started 2 min after initiation of handgrip exercise and 6 min after the end of dipyridamole infusion. The dynamic positron emission tomographic image acquisition followed the same protocol used in the baseline study.

Ammonia compartmental model. To describe the N-13 kinetic properties in myocardium observed in dynamic positron emission tomographic data, we developed a simple three compartment model that represents vascular and extravascular N-13 ammonia as well as metabolically trapped N-13 in the form of glutamine (Fig. 1). This model was developed under the following set of assumptions.

1) N-13 ammonia behaves like a freely diffusible tracer at the capillary-myocardial tissue interface.

2) N-13 ammonia is converted to N-13 glutamine by glutamine synthetase and is "essentially" trapped within the myocardial tissue.

3) The extracellular and intracellular N-13 ammonia pools rapidly equilibrate.

4) The available glutamine synthetase level remains essentially unchanged throughout the study and, therefore, the probability that an ammonia molecule in the tissue is converted to glutamine remains constant.

Components of the model. Given this set of assumptions, simple linear first order differential equations can be derived to describe the rate of change of N-13 concentration in each compartment of the model. The first compartment of this model represents the concentration of N-13 ammonia in arterial blood as a function of time ($C_a[t]$). The transport of N-13 ammonia between the vascular compartment and the extravascular N-13 ammonia compartment ($C_E[t]$) is represented by K_1 and k_2. This extravascular compartment is a conceptual construct used to represent the intracellular and extracellular N-13 ammonia in myocardial tissue. The third compartment of this model reflects N-13 ammonia that has

JACC Vol. 15, No. 5
April 1990:1032–42

Table 1. Symbols Used in the Model Equations

Symbol	Description	Units
$C_a(t)$	Arterial blood N-13 ammonia concentration	mCi/ml blood
$C_T(t)$	Total tissue N-13 concentration	mCi/g tissue
$C_E(t)$	N-13 ammonia concentration in tissue	mCi/g tissue
$C_G(t)$	N-13 glutamine concentration in tissue	mCi/g tissue
$C_m(t)$	Measured N-13 concentration	mCi/ml
$C_p(t)$	Measured tissue N-13 concentration	mCi/ml
K_1	Ammonia uptake rate	ml/g per min
k_2	Ammonia washout rate	min^{-1}
k_3	N-13 glutamine formation rate constant	min^{-1}
λ	N-13 decay constant	min^{-1}
ρ tissue	Tissue density	g tissue/ml tissue
t_1	Start scan time	min
t_2	End scan time	min
MBV	Fractional blood volume	ml blood/ml
MVV	Fractional blood volume spillover	ml blood/ml
TBV	Total fractional blood volume	ml blood/ml
F	Blood flow	ml/g per min
E	Extraction fraction	Unitless
PS	Permeability-surface area product	g-min/ml

been converted to N-13 glutamine by glutamine synthetase and is "essentially" trapped in the tissue ($C_G[t]$). The rate constant k_3 represents the conversion of N-13 ammonia into N-13 glutamine.

The following differential equations describe the rate of change in N-13 concentration in myocardial tissue as a function of time for each tissue compartment of the model:

$$\frac{dC_E(t)}{dt} = K_1C_a(t) - k_2C_E(t) - k_3C_E(t) - \lambda C_E(t) \quad [1]$$

$$\frac{dC_G(t)}{dt} = k_3C_E(t) - \lambda C_G(t). \quad [2]$$

The symbols used in the model equations are defined in Table 1. Each term on the right side of equations 1 and 2 represents the radionuclide flux (mCi/g tissue per min) across the boundaries of the conceptual compartmental model. Therefore, K_1 represents the combined processes of the delivery of the radionuclide to the tissue by blood flow and the extraction of the tracer across the capillary-tissue interface in a single capillary transit and must have units of ml blood/g tissue per min. The other constants of the model (k_2, k_3 and λ) are true rate constants (min^{-1}), reflecting the probability that a single radionuclide within a given conceptual compartment will either be lost by the system or moved to another compartment. Solution of equations 1 and 2 (see Appendix) yields a description of the concentration of N-13 in myocardial tissue as a function of time ($C_T[t]$).

$$C_T(t) = C_E(t) + C_G(t)$$

$$= \left[K_1e^{-(k_2+k_3+\lambda)t} + \frac{K_1k_3}{\alpha_2-\alpha_1}[e^{-\alpha_1 t} - e^{\alpha_2 t}]\right] \otimes C_a(t), \quad [3]$$

where

$$\alpha_{2,1} = \frac{(k_2 + k_3 + 2\lambda) \pm \sqrt{(k_2 + k_3 + 2\lambda)^2 - 4\lambda(k_2 + k_3 + \lambda)}}{2} \quad [4]$$

and $\otimes$ represents the mathematic operation of convolution (17).

Myocardial tissue concentrations. The measured activity in a single positron emission tomographic image frame does not represent the instantaneous radionuclide concentration in the tissue, but rather the integral of the activity from the beginning (t_1) to end (t_2) of the data acquisition within the volume of space represented by each image pixel. Therefore, the tissue radionuclide concentration measured with positron emission tomography ($C_p[t]$) must be corrected by the myocardial tissue density (ρ_{tissue}) and will be expressed as:

$$C_p(t) = \frac{\rho_{tissue}\int_{t_1}^{t_2} C_T(t)dt}{(t_2 - t_1)}. \quad [5]$$

In addition, the finite spatial resolution of positron emission tomography does not enable the delineation of myocardial tissue N-13 levels from vascular and ventricular N-13 levels. The positron emission tomographic measurement ($C_m[t]$) must, therefore, be described as the sum of the concentrations in the tissue and blood compartments:

$$C_m(t) = \frac{1}{(t_2 - t_1)}\left[(1 - MBV - MVV)\rho_{tissue}\int_{t_1}^{t_2} C_T(t)dt + MBV\int_{t_1}^{t_2} C_a(t)dt + MVV\int_{t_1}^{t_2} C_a(t)dt\right]. \quad [6]$$

In equation 6, MBV represents the blood volume in myocardial tissue divided by the physical measurement volume represented by the data, and MVV represents the fraction of the ventricular blood activity that spills over into tissue as a result of finite image resolution divided by the same physical measurement volume. It is important to note that the tissue ($C_T[t]$) and blood components ($C_a[t]$) of the measurement ($C_m[t]$) must be scaled by the fraction of the

measurement volume occupied by each component so that the radionuclide concentrations reflect the concentration within each tissue type rather than the radionuclide quantity of each tissue type divided by the total measurement volume. In equation 6, both the myocardial tissue blood volume (MBV) and the myocardial ventricular blood volume (MVV) are linear scale factors for the arterial blood curve and cannot be uniquely identified without additional measurements. In this application, we have chosen to lump both the spillover and myocardial blood volume factor into a single constant term that represents the total fractional blood volume (TBV). Thus, equation 6 can be reduced to the following expression:

$$C_m(t) = \frac{1}{(t_2 - t_1)} \left[(1 - TBV)\rho_{tissue} \int_{t_1}^{t_2} C_f(t)dt + TBV \int_{t_1}^{t_2} C_a(t)dt \right] \quad [7]$$

Myocardial blood flow calculations. In the previous description of the compartmental model, the constants K_1 and k_2, which describe the delivery and removal of myocardial N-13 ammonia, are related to both the flow of blood through the tissue and the mechanism for transport of ammonia between capillary blood and myocardial tissue. The influx of the tracer from the arterial blood into the myocardial tissue is given by the product of K_1 and the arterial blood concentration of the tracer. Closer examination of K_1 reveals that it must represent the product of the delivery of blood to the tissue or mass-specific blood flow (F) and the fraction of the tracer that traverses the capillary membrane and enters the myocardial tissue (single pass extraction fraction [E]). For freely diffusible tracers, Kety (18) has shown that the single pass extraction fraction can be calculated from the capillary permeability-surface area product and the mass-specific flow of blood through the tissue, as shown in equation 8:

$$K_1 = FE = F(1 - e^{-PS/F}). \quad [8]$$

Variable estimation. The attenuation-corrected images (128 × 128 matrix) were analyzed using a region of interest technique. With use of the last image frame (360 s), regions of interest were applied to the left ventricular chamber (12 pixels square) as well as to the lateral, anterior and septal walls of the left ventricle. These regions were subsequently copied to all acquired image frames, and regional time-activity curves were generated. Previous validation studies (19) have demonstrated a close agreement between the arterial input function obtained from the left ventricle region of interest with directly sampled arterial blood. Estimates of the variables of the ammonia compartmental model previously described (20) were obtained with a nonlinear least squares curve fitting algorithm based on the Marquardt algorithm.

Two specific configurations of the model (equation 7, were fit to the region of interest data from the lateral, anterior and septal walls of the left ventricle in each patient. In model *configuration I*, the value for the rate constant k_3 describing the metabolism of ammonia to glutamine was fixed at zero, and estimates for the total fractional blood volume, K_1, and k_2 were obtained. In *configuration II*, all four variables of the model (total fractional blood volume, K_1, k_2, k_3) were estimated. In each case, the Marquardt algorithm was modified to constrain all variable estimates to positive values. The results from each model configuration were examined in both the rest and dipyridamole data to assess the model configuration that can be supported by the kinetic behavior of ammonia in myocardial tissue and the statistical nature of the positron emission tomographic data.

Correction of arterial input function for N-13 metabolites. N-13 ammonia is rapidly metabolized to urea and glutamine in several organ systems (21,22). The arterial blood activity, therefore, represents a mixture of N-13–labeled ammonia, urea and glutamine. Accurate quantification of myocardial blood flow would ideally require the identification of the temporal and kinetic behavior of the metabolites in both the arterial blood and myocardial tissue. We recently described (23) the behavior of N-13 ammonia metabolites in the blood in a series of healthy human volunteers. Therefore, we have attempted to account for the blood metabolites in the kinetic model. The input function was corrected for the mean levels of metabolites observed in the healthy volunteers. The blood spillover contribution was incorporated as the sum of all N-13 ammonia levels in the blood. Results with and without correction for metabolites were then compared in an attempt to gauge the importance of this correction on the estimation of myocardial blood flow with N-13 ammonia.

Results

Hemodynamic response to dipyridamole. Dynamic positron emission tomography studies at baseline and after infusion of dipyridamole were completed in seven healthy volunteers. Systolic blood pressure and heart rate averaged 122 ± 11 mm Hg and 68 ± 6 beats/min, respectively. After dipyridamole infusion and handgrip exercise, systolic blood pressure increased to 128 ± 14 mm Hg (p = NS) and heart rate to 92 ± 12 beats/min ($p < 0.01$ versus baseline). No subject developed nausea, chest pain or bronchoconstriction after intravenous infusion of dipyridamole.

Kinetic behavior of ammonia in myocardium. Figure 2 shows dynamic positron emission tomographic images at rest and after dipyridamole infusion in one subject. The temporal resolution of the image acquisition demonstrates the kinetic behavior of N-13 ammonia as it traverses the right ventricle, lungs and left ventricle. As the study proceeds, the uptake and retention of the tracer in the myocardium is observed as the blood radioactivity clears. After dipyridamole infusion, the myocardium to background N-13 ammo-

JACC Vol. 15, No. 5
April 1990:1032–42

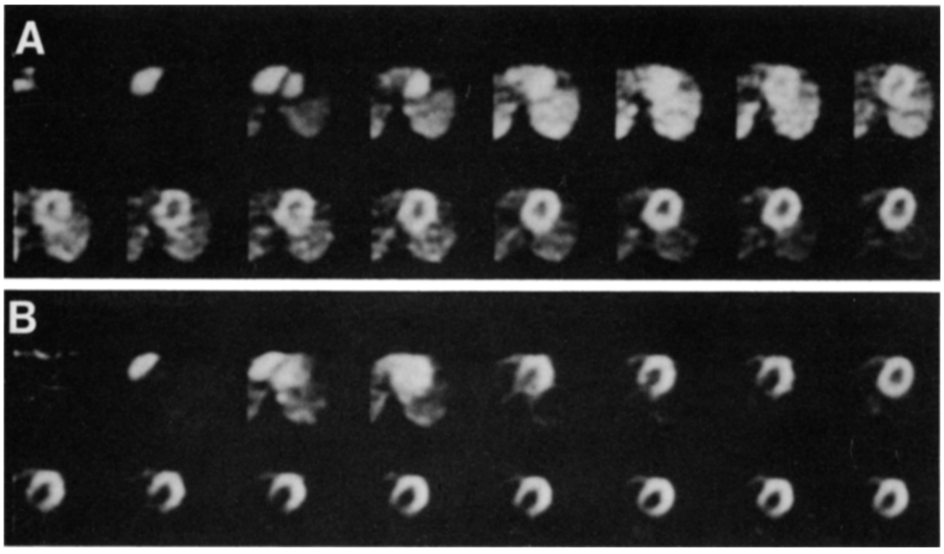

Figure 2. Serial cross-sectional positron emission tomographic images through the left ventricle obtained at baseline (A) and after dipyridamole infusion (B). Initially, N-13 ammonia concentrates in the right and left ventricular chambers. The later images represent retention of N-13 ammonia in the myocardium.

nia ratio clearly demonstrates the increased uptake of the tracer at high flow rates.

An example of regional time-activity curves generated by placing a region of interest over the wall of the left ventricle and left ventricular chamber for a rest and dipyridamole study are shown in Figure 3. The concentration of N-13 ammonia levels increases rapidly as the bolus of activity in the blood transverses the tissue (approximately 2 min). The myocardial N-13 ammonia level reaches a plateau after the initial bolus and remains constant throughout the remainder of the study. The uptake and retention of N-13 ammonia increase markedly after dipyridamole infusion. The concentration of N-13 ammonia measured over the final 360 s of each study normalized by the integral of the N-13 ammonia blood concentration averaged 1.96 ± 0.6 times higher than the baseline level when dipyridamole was administered.

Figure 3. Left, Baseline time-activity curves obtained from a region of interest placed over the left ventricular chamber (**circles**) and myocardial regions (**squares**). **Right,** Results after dipyridamole infusion in the same patient.

Estimates of myocardial blood flow. Myocardial blood flow was estimated by fitting model configurations I and II to the time-activity curves for each patient (see Methods). The mean value ± SD of each rate constant for both model configurations are presented in Table 2. The differences between the model fit and measured data for the lateral wall region of interest as a function of time—called residuals—in each patient are shown in Figure 4. Curves A and B represent the residuals for the rest studies using model configurations I and II, respectively. The behavior of these residuals was very similar, with the exception of the last time point of the imaging sequence. This small bias in the residuals about zero was essentially eliminated when k_3 is added to the conceptual model. Curves C and D in Figure 4 represent the residuals for the dipyridamole studies using model configurations I and II, respectively. Again, the behavior of the residuals was similar, with the exception of the late data points. Addition of k_3 to the model for the vasodilation studies essentially eliminated large residuals in the tail of the fit. However, the additional term in the model did not eliminate serial correlation patterns through the early

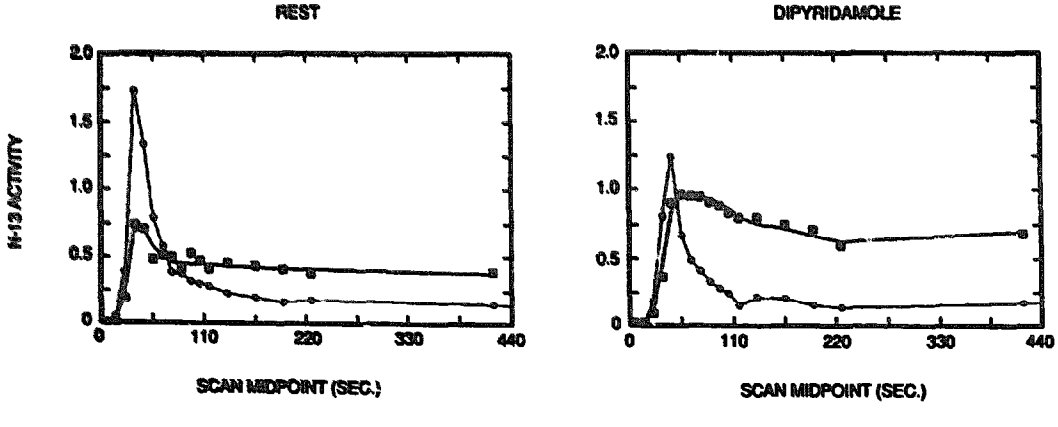

Table 2. Mean and Standard Deviation of Individual Rate Constants Using Model Configurations I and II and Correction for N-13 Metabolites in Blood

	K_1	k_2	k_3
Model I			
Baseline	0.83 ± 0.19	0.18 ± 0.09	—
Dipyridamole	3.95 ± 1.5	0.65 ± 0.42	—
Model II			
Baseline	0.88 ± 0.17	0.29 ± 0.13	0.11 ± 0.05
Dipyridamole	4.17 ± 1.1	1.26 ± 0.70	0.19 ± 0.04

Table 3. Mean and Standard Deviation of Individual Rate Constants With (C) and Without (NC) Correction for N-13 Metabolites in Blood Using Model Configuration II

	K_1 (ml/min per g)	k_2 (min^{-1})	k_3 (min^{-1})	CR
Baseline				
C	0.88 ± 0.17	0.29 ± 0.13	0.11 ± 0.05	—
NC	0.81 ± 0.15	0.33 ± 0.15	0.03 ± 0.03	—
Dipyridamole				
C	4.17 ± 1.1	1.26 ± 0.70	0.19 ± 0.04	4.8 ± 1.3
NC	3.90 ± 1.1	1.18 ± 0.72	0.08 ± 0.04	4.7 ± 1.4

CR = coronary reserve.

and middle time period of the study. Potential explanations for this behavior are presented in the Discussion section.

Effect of correction for metabolites on flow determination. To evaluate the effect of the correction for N-13 metabolites in blood on myocardial blood flow and rate constant estimates, the results of the curve fitting with and without a correction factor for N-13 ammonia metabolism were compared. Table 3 depicts the individual rate constants derived from both curve fitting procedures. Estimates of K_1 and k_2 were only slightly influenced by N-13 metabolites in blood (<10%), whereas k_3 was three times larger at baseline and two times larger after dipyridamole infusion when metabolites were considered in the fitting procedure. The coronary reserve defined by the ratio of dipyridamole flow to rest flow was not affected by the correction for metabolites (Table 3).

Figure 5 shows plots of the rate constant estimates for each region of interest in each patient for both the rest (squares) and dipyridamole (circles) studies. The closed symbols represent rate constants calculated using a blood curve with metabolite correction, and the open symbols represent those calculated without metabolite correction. The solid lines on each plot represent the mean values presented in Table 3. These data demonstrate that the major effect of metabolite correction was on the estimate of k_3. The model variables K_1 and k_2 exhibited only minor deviations when the metabolite corrections were included.

Coronary flow reserve. Figure 6 shows a bar graph representing the mean coronary flow reserve calculated on the

Figure 4. Residuals between model fit and measured data for all lateral wall regions of interest analyzed. **Panels A** and **B** represent the residuals for model configuration I and II fits to the rest studies, respectively. **Panels C** and **D** represent the residuals for model configuration I and II fits to the dipyridamole studies, respectively. The data points at each abscissa represent the difference between the model function and the measured data at that specific time in the study.

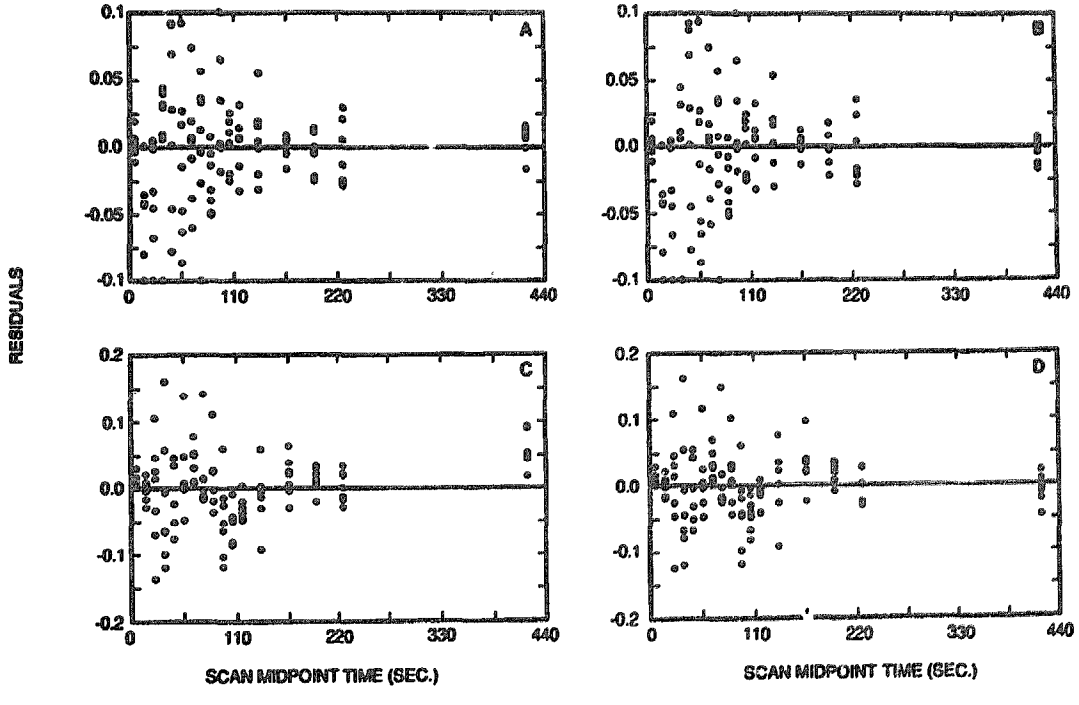

JACC Vol. 15, No. 5
April 1990:1032–42

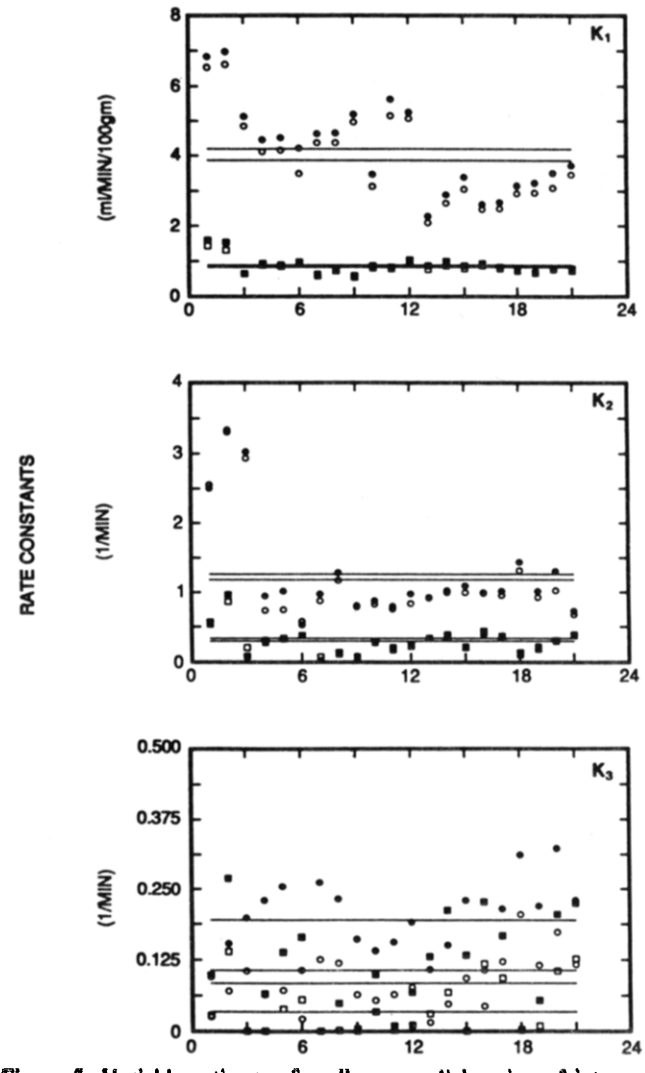

Figure 5. Variable estimates for all myocardial region of interest data analyzed in this study. Each plot represents individual variable estimates (K_1, **top**; k_2, **center**; k_3, **bottom**) for model configuration II fits to the data. In all plots, **circles** represent dipyridamole (DIP) studies and **squares** represent the rest studies. The **closed symbols** are for fitting procedures using metabolite-corrected blood curves, and **open symbols** represent analysis without metabolic corrections.

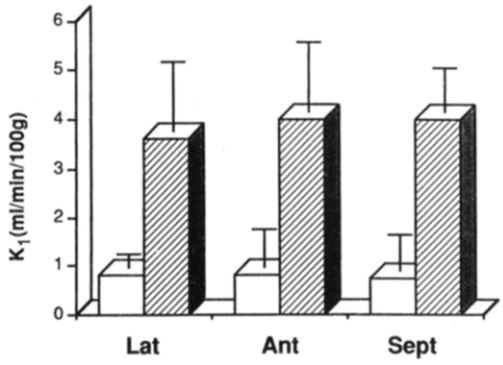

Figure 6. Regional blood flow values (K_1) at baseline (open bars) and after infusion of dipyridamole (Dip) (hatched bars) derived from regions of interest placed over septal (Sept), anterior (Ant) and lateral (Lat) walls of the left ventricle.

basis of K_1 estimates for each segment of the left ventricle analyzed. The results show a mean coronary flow reserve of 4.8 ± 1.3. Figure 6 shows that the coronary flow reserve was homogeneous throughout the left ventricular myocardium.

Discussion

Validity of the method. The data presented in this report demonstrate the feasibility of estimating regional myocardial perfusion in the human heart with N-13 ammonia and dynamic positron emission tomographic imaging. By using a simple conceptual three compartment tracer kinetic model, isolation of the initial extraction of tracer by the tissue from subsequent metabolic radionuclide trapping in the form of N-13 glutamine can be achieved. The kinetic model variable K_1, which represents the delivery and extraction of N-13 ammonia, can be used as an estimate of myocardial blood flow as long as the single pass extraction fraction is high (that is, the permeability-surface area product is large relative to blood flow). The magnitude of rest and dipyridamole flow values observed in this study suggests the validity of the model. The measured coronary reserve of 4.8 ± 1.3 in normal volunteers agrees closely with results obtained by a variety of other independent techniques (24,25).

There was no direct validation of the positron emission tomographic flow data by comparison with invasive flow measurements in this study. Invasive procedures such as digital angiography, thermodilution or Doppler flow catheters assess blood flow velocity in large epicardial arteries (25–27). Estimates of flow velocity correlate with myocardial perfusion, but do not provide accurate flow estimates without assessing the tissue mass being perfused by a given coronary artery. Therefore, the validation of positron emission tomographic measurements in the human heart by independent methods based on velocity measurements in epicardial arteries may be limited and was not attempted in this study.

N-13 ammonia as a flow tracer. The "ideal" blood flow tracer is expected to be highly extracted by the myocardium and its tissue retention to be linearly related to flow over a wide range. Radiolabeled microspheres fulfill these criteria, with nearly 100% extraction by the tissue, which is independent of the flow state (8,28). However, the need for arterial injection of this tracer limits its clinical use. O-15 water is highly extracted by tissue and can be used as an intravenously injected flow tracer (7,9,10,29). However, this tracer is freely diffusible across membranes, which results in rapid clearance kinetics from myocardium and only little contrast between blood and tissue activity. Application of O-15 water for the evaluation of myocardial blood flow by positron emission tomography requires delineation of blood activity

by an independent tracer method to define myocardial tissue (10). These more complex imaging protocols limit the feasibility of this approach as a routine clinical procedure.

The flow tracer N-13 ammonia represents a compromise between microspheres and freely diffusible tracers such as O-15 water. This tracer is highly extracted by the myocardium and is retained in tissue in proportion to blood flow (6,15,30). The internal exchange of ammonia between vascular and extravascular space in the myocardium is determined by diffusion, whereas retention involves the metabolic trapping of N-13 ammonia in the form of N-13 glutamine (6). Previous criticism (15) of the use of N-13 ammonia as a flow tracer focused on this metabolic component of activity retention. Myocardial retention of N-13 ammonia can be altered by pharmacologic inhibition of glutamine synthesis. Therefore, retention of N-13 ammonia may represent a combination of blood flow and the metabolic state of the myocardium. At high flow states, "metabolic trapping" of N-13 ammonia becomes the rate-limiting step of tracer retention. This leads to an underestimation of blood flow in the high flow state, limiting previous attempts (14) to accurately assess blood flow in the high flow states.

N-13 ammonia extraction. To overcome this limitation in assessing blood flow in the high flow state, a tracer kinetic approach was developed to separate extraction from retention. In the proposed model, K_1 represents the product of blood flow and extraction fraction of the tracer. The first pass extraction of N-13 ammonia has not been determined in the human heart. However, animal studies (6) relating extraction of N-13 ammonia to microsphere blood flow measured in canine myocardium over a wide range of blood flow indicate a first pass extraction fraction >90%. Using the relation of blood flow times first pass extraction fraction assessed in canine myocardium by Schelbert et al. (6), the permeability surface (PS) area product for N-13 ammonia can be expressed as a function of blood flow (F):

$$PS = 108 + 2.34\ F \qquad [9]$$

Calculations of the extraction fraction over the flow range observed in our study predict a decrease in the extraction fraction to only 92% (measured flow [F] 460 ml/min per 100 g). Thus, blood flow will be only slightly underestimated on the basis of K_1 measurements of the kinetic model. This assumption is confirmed by the magnitude of coronary reserve calculated in the studied volunteers. The average value of 4.8 closely agrees with measurements based on relative changes in blood flow velocity assessed by Doppler flow catheter. Rossen et al. (24) reported a coronary reserve of 4.4 ± 1.1 obtained with intravenous injection of papaverine in patients with normal coronary arteries.

Compartmental model configuration. The results of the curve fit residuals shown in Figure 4 demonstrate the validity of this model to describe the N-13 ammonia kinetics. With the limited temporal resolution of data acquisition possible with positron emission tomographic imaging, many myocardial time-activity curves at baseline could be adequately described by model configuration I, which did not incorporate k_3. This can be explained by noise in positron emission tomographic data and the slow trapping process of N-13 ammonia in myocardial tissue. Because data acquisition was limited to 10 min, model configuration I fit the baseline data because it increases the distribution volume of the extravascular compartment ($C_E[t]$) in the model by decreasing the k_2 estimate to account for the metabolically retained N-13 ammonia. However, the kinetic behavior of N-13 ammonia in the myocardial extravascular compartment is dramatically altered during high flow states (that is, a fourfold increase in K_1 and k_2). Under this condition, the concentration of N-13 ammonia is more rapidly cleared from the extravascular compartment, and the fitting procedure can no longer adjust to describe this behavior without the addition of k_3. Therefore, model configuration II is the most appropriate form of the model to describe the N-13 ammonia kinetics over a wide range of flow values (Fig. 4). Although model configuration I appeared adequate to describe the data at baseline study, model configuration II, which includes k_3 as a variable, produced "essentially" identical estimates of the total fractional blood volume, K_1, and k_2 with k_3 values near zero.

Metabolic correction of N-13 blood activity. N-13 ammonia is rapidly metabolized in several organs (21,22). Therefore, a correction factor for the contamination of the arterial input function by N-13 metabolites was applied. The data in this study demonstrate that the blood flow values (K_1 estimates) show only a slight dependence on N-13 metabolites because K_1 estimates are primarily dependent on the tracer kinetics during the first 2 min after injection of N-13 ammonia. At this time, little metabolic contamination of the arterial input function has been observed (22). The coronary reserve measurement did not change after correction for metabolites, indicating the clinical practicability of the positron emission tomography approach without the need for N-13 metabolite correction. However, k_3 is sensitive to the N-13 metabolite correction. Therefore, kinetic positron emission tomographic studies evaluating the rate of metabolic incorporation of N-13 ammonia require correction of the arterial input function for N-13 metabolites.

Limitations to quantification. The major limitation of all quantitative techniques for examination of the human heart with positron emission tomography results from the limited resolution of the instrumentation and motion of the heart through the cardiac cycle. Recently, Iida et al. (31) addressed this issue by applying a technique that estimates myocardial blood flow from the washout rate of O-15 water from the tissue after a bolus administration. Because the rate at which radioactivity egresses from the tissue is not proportional to the geometry of the tissue relative to the image plane of the tomograph, this technique will be insensitive to

JACC Vol. 15, No. 5
April 1990:1032–42

partial volume distortions (32). However, examination of the error properties for dynamic O-15 water techniques in the brain, as demonstrated by Koeppe et al. (33), shows that the coefficient of variation for model washout variables is much larger than the coefficient of variation of K_1, the model variable describing the uptake of tracer. Therefore, studies designed to examine the relative change in myocardial blood flow when comparing physiologic states are more effective using estimates of the uptake variable rather than the washout model variables. Conversely, the development of studies that rely on a single absolute estimate of myocardial blood flow may be more appropriately suited for a technique that is free of partial volume distortions. In the present study, this technique was developed for the estimation of coronary reserve, which reflects relative changes of flow and is, therefore, less sensitive to partial volume effects.

The data presented here were obtained in healthy volunteers. Further studies are required to assess the error sensitivity of the proposed approach in patients with coronary artery disease. Blood flow reduction may be more difficult to accurately assess. Low count statistics and geometric factors (wall thinning) may limit the application of this approach under such circumstances (32,34).

Conclusions. Dynamic positron emission tomographic imaging with N-13 ammonia allowed the quantitative assessment of myocardial blood flow at rest and after intravenous infusion of dipyridamole; the data agreed well with those obtained by independent techniques such as digital angiography and Doppler catheter estimates. With use of a new tracer kinetic model, N-13 ammonia extraction can be separated from the metabolic N-13 ammonia tissue retention. Blood flow measurements based on N-13 ammonia extraction are more accurate at high flow states and less sensitive to potential changes in the metabolic environment.

This study demonstrates the feasibility of noninvasive quantitation of the regional coronary reserve by using positron emission tomography, which will allow assessment of the functional significance of regional coronary artery disease and evaluation of vascular conductance in various cardiac diseases. Further clinical studies in patients with coronary artery disease will determine the diagnostic value of quantitative flow measurements for assessing the severity of coronary artery disease. Thus, positron emission tomography may be a clinically useful tool to objectively define the significance of disease and may provide absolute flow criteria to optimize therapy and study the effect of coronary interventions.

Appendix

The kinetic model describing the behavior of N-13 ammonia in myocardial tissue is based on the following assumptions:

1) N-13 ammonia behaves like a freely diffusible tracer at the capillary-myocardial tissue interface.

2) N-13 ammonia is converted to N-13 glutamine by glutamine synthetase and is "essentially" trapped within the myocardial tissue.

3) The extracellular and intracellular N-13 ammonia pools rapidly equilibrate.

4) The available glutamine synthetase level remains essentially unchanged throughout the study and, therefore, the probability that an ammonia molecule in the tissue is converted to glutamine remains constant.

These simple assumptions lead to a set of linear first order differential equations describing the kinetics observed in myocardial tissue (see Table 1 for abbreviations):

$$\frac{dC_E(t)}{dt} = K_1C_a(t) - k_2C_E(t) - k_3C_E(t) - \lambda C_E(t) \quad [1a]$$

$$\frac{dC_G(t)}{dt} = k_3C_E(t) - \lambda C_G(t). \quad [2a]$$

A solution to this set of coupled differential equations can be derived using Laplace transform techniques (35). The first step in the derivation consists of taking the Laplace transform of equations 1a and 2a:

$$sC_E(s) - C_E(0) = K_1Ca(s) - k_2C_E(s) - k_3C_E(s) - \lambda C_E(s) \quad [3a]$$

$$sC_G(s) - C_G(0) = k_3C_E(s) - \lambda C_G(s). \quad [4a]$$

Algebraic manipulation of each of these equations, assuming that initial tracer concentrations in the tissue are zero, leads to the following expressions:

$$C_E(s) = \frac{K_1C_a(s)}{s + k_2 + k_3 + \lambda} \quad [5a]$$

$$C_G(s) = \frac{k_3C_E(s)}{s + \lambda}. \quad [6a]$$

Substitution of equation 5a into equation 6a yields:

$$C_G(s) = \frac{K_1k_3C_a(s)}{(s + \lambda)(s + k_2 + k_3 + \lambda)}. \quad [7a]$$

Equations 5a and 7a can now be inverse Laplace-transformed to form an expression for the radionuclide concentration in each tissue compartment as a function of time. Equation 5a is easily separated into the product of two functions $C_a(s)$ and $K_1/(s + k_2 + k_3 + \lambda)$. Therefore, the expression for $C_E(t)$ will be the convolution of the inverse transform of each of these functions:

$$L^{-1}(C_a(s)) = C_a(t) \quad [8a]$$

$$L^{-1}(K_1/(s + k_2 + k_3 + \lambda)) = K_1e^{-(k_2 + k_3 + \lambda)t}. \quad [9a]$$

Therefore:

$$C_E(t) = K_1e^{-(k_2 + k_3 + \lambda)t} \otimes C_a(t) \quad [10a]$$

Because the arterial input curve $C_a(t)$ will vary from patient to patient or study to study, it cannot be described explicitly through the use of an equation.

Inverse transformation of equation 7a is a little more complex because it does not cast itself into a form that is easily transformed. However, if the two terms in the denominator of this expression are multiplied, a quadradic function of s is produced:

$$(s + \lambda)(s + k_2 + k_3 + \lambda) = s^2 + s \cdot (k_2 + k_3 + 2\lambda) + \lambda(k_2 + k_3 + \lambda). \quad [11a]$$

It is easy to show that the roots (α_1, α_2) of this expression are

$$\alpha_{2,1} = \frac{(k_2 + k_3 + 2\lambda) \pm \sqrt{(k_2 + k_3 + 2\lambda)^2 - 4\lambda(k_2 + k_3 + \lambda)}}{2}. \quad [12a]$$

Thus, equation 7a can be expressed in a form for which the inverse Laplace transform can be calculated:

$$C_G(s) = \frac{K_1 k_3 C_a(s)}{(s - \alpha_1)(s - \alpha_2)}. \quad [13a]$$

Once again, the expression in equation 13a is the product of two functions for which the inverse transform can be calculated easily:

$$L^{-1}(C_a(s)) = C_a(t) \quad [14a]$$

$$L^{-1}\left(\frac{K_1 k_3}{(s - \alpha_1)(s - \alpha_2)}\right) = \frac{K_1 k_3}{\alpha_2 - \alpha_1}[e^{-\alpha_1 t} - e^{-\alpha_2 t}]. \quad [15a]$$

The expression for $C_G(t)$ then becomes the convolution of the functions in equations 14a and 15a:

$$C_G(t) = \frac{K_1 k_3}{\alpha_2 - \alpha_1}[e^{-\alpha_1 t} - e^{-\alpha_2 t}] \otimes C_a(t). \quad [16a]$$

Summation of equations 10a and 16a then produce an expression for the tissue radionuclide concentration:

$$C_T(t) = K_1 e^{-(k_2 + k_3 + \lambda)t} \otimes C_a(t) + \frac{K_1 k_3}{\alpha_2 - \alpha_1}[e^{-\alpha_1 t} - e^{-\alpha_2 t}] \otimes C_a(t). \quad [17a]$$

We thank Ron Sumida, Cynthia Witt and Francine Aguilar for technical assistance obtaining the positron emission tomographic studies, and J. Bida, PhD and Joseph Cook for production of the isotopes. We thankfully appreciate the secretarial assistance of Jill Anderson in preparing the manuscript.

References

1. Marcus ML, Wilson RF, White CW. Methods of measurement of myocardial blood flow in patients: a critical review. Circulation 1987;76:245–53.
2. Strauss HW, Harrison K, Langan J, Lebowitz E, Pitt B. Thallium-201 for myocardial imaging: relation of thallium-201 to regional myocardial perfusion. Circulation 1975;51:641–5.
3. Vandeberg BF, Kieso R, Fox-Eastham K, Chilian W, Kerber RE. Quantitation of myocardial perfusion by contrast echocardiography: analysis of contrast gray level appearance variables and intracyclic variability. J Am Coll Cardiol 1989;13:200–6.
4. Rumberger JA, Feiring AJ, Lipton MJ, Higgins CB, Ell SR, Marcus ML. Use of ultrafast computed tomography to quantitate regional myocardial perfusion: a preliminary report. J Am Coll Cardiol 1987;9:59–69.
5. LeGrand V, Mancini GBJ, Bates ER, Hodgson JMcB, Gross MD, Vogel RA. Comparative study of coronary flow reserve, coronary anatomy and results of radionuclide exercise tests in patients with coronary artery disease. J Am Coll Cardiol 1986;8:1022–32.
6. Schelbert HR, Phelps ME, Huang S-C, et al. N-13 ammonia as an indicator of myocardial blood flow. Circulation 1981;63:1259–72.
7. Huang SC, Schwaiger M, Carson RE, Carson J, Phelps ME, Schelbert HR. Quantitative measurement of myocardial blood flow with oxygen-15 water and positron computed tomography: an assessment of potential and problems. J Nucl Med 1985;25:616–25.
8. Wisenberg G, Schelbert HR, Hoffman EJ, et al. In vivo quantitation of regional myocardial blood flow by positron-emission computed tomography. Circulation 1981;63:1248–58.
9. Bergman SR, Fox KA, Rand AL, et al. Quantification of regional myocardial blood flow in vivo with $H_2{}^{15}O$. Circulation 1984;70:724–33.
10. Knabb RM, Fox KA, Burton CB, Sobel BE, Bergman SR. Characterization of the functional significance of subcritical coronary stenoses with $H_2{}^{15}O$ and positron-emission tomography. Circulation 1985;71:1271–8.
11. Schelbert HR, Phelps ME, Hoffman EJ, Huang S-C, Selin CE, Kuhl DE. Regional myocardial perfusion assessed with N-13 labeled ammonia and positron emission computerized axial tomography. Am J Cardiol 1979;43:209–18.
12. Tamaki N, Yonekura Y, Senda M, et al: Myocardial positron computed tomography with ^{13}N-ammonia at rest and during exercise. Eur J Nucl Med 1985;11:246–51.
13. Gould KL, Goldstein RA, Millani NA, et al. Non-invasive assessment of coronary stenosis by myocardial perfusion imaging during pharmacologic coronary vasodilation. VIII. Clinical feasibility of positron cardiac imaging without a cyclotron using generator-produced rubidium-82. J Am Coll Cardiol 1986;7:775–89.
14. Shah A, Schelbert HR, Schwaiger M, Hansen H, Selin C. Measurement of regional myocardial blood flow with N-13 ammonia and positron-emission tomography in intact dogs. J Am Coll Cardiol 1985;5:92–100.
15. Bergman ST, Hack S, Tewson T, Welch MJ, Sobel BE. The dependence of accumulation of $^{13}NH_3$ by myocardium on metabolic factors and its implications for the quantitative assessment of perfusion. Circulation 1978;61:34–41.
16. Brown BG, Josephson MA, Peterson RB, et al. Intravenous dipyridamole combined with isometric handgrip for near maximal acute increase in coronary flow in patients with coronary artery disease. Am J Cardiol 1981;48:1077–85.
17. Bracewell RN. The Fourier Transform and its Applications. 2nd ed. New York: McGraw-Hill, 1978:24–50.
18. Kety SS. The theory and applications of the exchange of inert gas at the lungs and tissues. Pharmacol Rev 1951;3:1–41.
19. Gambhir SS, Schwaiger M, Huang S-C, et al. A simple non-invasive quantification method for measuring myocardial glucose utilization in humans employing positron emission tomography and ^{18}F-deoxyglucose. J Nucl Med 1989;30:359–66.
20. Marquardt DW. An algorithm for least-squares estimation of non-linear parameters. J Soc Indust Appl Math 1963;11:431–41.
21. Rosenspire KC, Gelbard AS, Cooper AJT, Schmid FA, Roberts J. [N-13] Ammonia and L-[amide] N-13 glutamine metabolism in glutaminase-sensitive and glutaminase-resistant murine tumors. Biochem Biophys Acta 1985;843:37–48.
22. Cooper AJL, Nieves E, Coleman AE, Filc-DeRicco S, Gelbard AS. Short-term metabolic rate of [N-13] ammonia in rat liver in vivo. J Biol Chem 1987;262:1073–80.
23. Rosenspire KC, Schwaiger M, Mangner TJ, Hutchins GD, Sutorik A, Kuhl DE. Metabolic fate of N-13 ammonia in human and canine blood. J Nucl Med (in press).
24. Rossen JD, Simonetti I, Marcus ML, Winniford MD. Coronary dilation with standard dose dipyridamole and dipyridamole combined with handgrip. Circulation 1989;79:566–72.
25. Wilson RF, Laughlin DE, Ackell PH, et al. Transluminal subselective measurement of coronary artery blood flow velocity and vasodilator reserve in man. Circulation 1985;72:82–92.

26. Bagger JP. Coronary sinus blood flow determination by the thermodilution technique: influence of catheter position and respiration. Cardiovasc Res 1984;19:27–31.

27. Hodgson JMcB, LeGrand V, Bates ER, et al. Validation in dogs of a rapid digital antiographic technique to measure relative coronary blood flow during routine cardiac catheterization. Am J Cardiol 1985;55:188–93.

28. Heymann MA, Payne BD, Hoffman JIE, Rudolph AM. Blood flow measurements with radionuclide-labeled particles. Prog Cardiovasc Dis 1977;20:55–79.

29. Raichle ME, Eichling JO, Straatmann MG, Welch MJ, Larson KB, Ter-Pogossian MM. Blood-brain barrier permeability of ^{11}C-labeled alcohols and ^{15}O-labeled water. Am J Physiol 1976;230:543–52.

30. Endo M, Yoshida K, Iinuma TA, et al. Noninvasive quantification of regional myocardial blood flow and ammonia extraction fraction using nitrogen-13 ammonia and positron emission tomography. Ann Nucl Med 1987;1:1–6.

31. Iida H, Kanno I, Takahashi A. Measurement of absolute myocardial blood flow with H_2O-15 and dynamic positron-emission tomography. Circulation 1988;78:104–15.

32. Hoffman EJ, Huang SC, Phelps ME. Quantitation in positron emission computed tomography. I. Effect of object size. J Comput Assist Tomogr 1979;3:299–308.

33. Koeppe RA, Holden JE, Ip WR. Performance comparison of parameter estimation techniques for the quantitation of local cerebral blood flow by dynamic positron computed tomography. J Cereb Blood Flow Metabol 1985;5:224–34.

34. Henze E, Huang SC, Ratib O, et al. Measurements of regional tissue and blood-pool radiotracer concentrations from serial tomographic images of the heart. J Nucl Med 1983;24:987–96.

35. Abramowitz M, Stegun IA. Handbook of Mathematical Functions. New York: Dover Publications, 1972:1019–29.